NextGen Scientific Publication
American International Journal of Computer Science and Technology

Volume 6 Issue 4, Pg. No. 84-92, AIJCST-V6I4P108, 2024
https://doi.org/10.63282/3117-5481/AIJCST-V6I4P108

Original Article

RF Shielding in Mission-Critical Infrastructure: Design, Installation, and Field-Level Optimization Techniques

***Yevhen Kidyaykin**
CEO at EKid.

Abstract:

This paper presents a design framework for hybrid radio-frequency (RF) and acoustic shielding systems intended for mission-critical infrastructure environments. A layered shielding architecture is proposed that integrates electromagnetic (EM) attenuation layers with acoustic isolation composites, and the predicted performance of that architecture is derived analytically using established shielding theory and the transfer matrix method. Under the material parameters adopted here, the modelled architecture yields shielding effectiveness above 100 dB across 14 kHz to 18 GHz together with acoustic isolation in the STC 55 class. A multi-objective optimization methodology combining genetic algorithms with particle swarm optimization is proposed for material selection and layer sequencing; applied to the modelled design space, it returns a 18.4% reduction in modelled installed cost relative to a conventional single-modality baseline. All numerical results in this paper are analytical predictions computed from published material properties and cost data. They are not field measurements, and no facility measurement campaign underlies them. Experimental validation of the modelled architecture is identified as the necessary next step.

Keywords:

RF Shielding, Electromagnetic Compatibility, Mission-Critical Infrastructure, SCIF, Hybrid Shielding, Acoustic Isolation, Shielding Effectiveness, Field Optimization, IEEE 299, Penetration Management.

Article History:

Received: 30.05.2024

Revised: 28.06.2024

Accepted: 06.07.2024

Published: 19.07.2024

I. Introduction

The proliferation of sophisticated electromagnetic threats ranging from intentional electromagnetic interference (IEMI) to high-altitude electromagnetic pulse (HEMP) events has elevated radio-frequency shielding from a recommended practice to an operational imperative for mission-critical infrastructure worldwide. Government facilities processing classified information, military command and control centers, critical healthcare installations housing sensitive diagnostic equipment, and financial data centers supporting high-frequency trading operations all share a common vulnerability: susceptibility to electromagnetic disruption that can compromise data integrity, operational continuity, and in extreme scenarios, human safety. Contemporary RF shielding practice faces a fundamental engineering tension. Single-modality shielding solutions optimized for electromagnetic attenuation often neglect the acoustic transmission pathways that can serve as both information leakage channels and structural coupling vectors for vibro-electromagnetic interference. The recognition that acoustic energy can modulate electromagnetic emissions through microphonic effects in cables and piezoelectric coupling in printed circuit board substrates has driven research toward integrated protection paradigms. However, the existing literature treats electromagnetic and acoustic shielding as largely independent disciplines, with few systematic investigations of their synergistic integration.

This paper addresses that gap by presenting a unified design framework for hybrid acoustic-electromagnetic shielding systems, developed analytically and exercised across five representative mission-critical facility categories defined as modelling scenarios. The principal contributions are threefold: (1) a layered composite shielding architecture predicted to achieve broadband SE above 100 dB with concurrent STC 55-class acoustic isolation; (2) a multi-objective optimization methodology for material selection and layer sequencing that reduces modelled installed cost by 18.4% relative to a conventional baseline design; and (3) a degradation and maintenance model that quantifies the lifecycle implications of gasket material selection. The facility categories are analytical scenarios rather than instrumented installations. The remainder of this paper is organized as follows. Section II reviews the theoretical foundations and relevant standards. Section III presents the hybrid shielding architecture and material characterization. Section IV details the optimization framework. Section V describes installation methodology and quality assurance protocols. Section VI presents the modelled performance of the architecture and the protocol by which it should be verified. Section VII discusses long-term performance and maintenance. Section VIII concludes with future research directions.

2. Theoretical Background and Standards Framework

2.1. Electromagnetic Shielding Theory

The shielding effectiveness of a planar barrier is classically decomposed into three loss mechanisms: reflection loss (R), absorption loss (A), and multiple internal reflection correction (M). For a single homogeneous layer, the total SE in decibels is expressed as:

$$SE(dB) = R + A + M = 20\log_{10}|(Z_0 + Z_s)^2 / 4Z_0Z_s| + 20\log_{10}|e^\wedge(\gamma t)| + 20\log_{10}|1 - e^\wedge(-2\gamma t)(Z_s - Z_0)^2/(Z_s + Z_0)^2|$$

Where Z_0 is the free-space impedance (377 Ω), Z_s is the shield impedance, γ is the propagation constant, and t is the material thickness. For electrically thin shields ($t << \delta$, the skin depth), reflection loss dominates at low frequencies, while absorption loss governs high-frequency performance. This frequency-dependent behavior necessitates multi-layer designs for broadband protection requirements.

For multi-layer composite shields, the transfer matrix method (TMM) provides an exact analytical framework. Each layer i is characterized by its 2×2 transmission matrix T_i, and the overall shield response is the cascaded product $T_{total} = \prod T_i$. This formalism naturally accommodates the hybrid acoustic-electromagnetic designs proposed in this work, where viscoelastic damping layers and air gaps are modeled as impedance discontinuities.

2.2. Acoustic Shielding Fundamentals

Acoustic isolation in shielded enclosures is governed by the mass law at frequencies below the critical coincidence frequency. The sound transmission loss (TL) of a single panel of surface density m (kg/m^2) at frequency f is approximated as:

$$TL(dB) \approx 20\log_{10}(\pi fm/\rho_0 c_0) - 5$$

Where ρ_0 and c_0 are the density and speed of sound in air. The mass law predicts approximately 6 dB of additional TL per doubling of either mass or frequency. However, at the coincidence frequency f_c, bending wave coupling causes a pronounced dip in TL—a phenomenon exploitable through constrained-layer damping in the hybrid designs described in Section III.

2.3. Applicable Standards and Compliance

Mission-critical RF shielding systems must satisfy a matrix of standards and criteria that varies by application domain, and the relationship between these instruments is frequently misstated in the applied literature. IEEE Std 299-2006 defines the measurement methodology for the shielding effectiveness of enclosures across 9 kHz to 18 GHz, extending beyond that range only under the additional conditions specified in the standard [1]. NSA/CSS Evaluated Products List 73-04 identifies shielded enclosure products that have been evaluated against NSA/CSS criteria; it is a product list from which designers select, not a facility shielding-performance standard, and it does not itself establish minimum SE requirements for SCIFs [4]. Facility RF shielding requirements for a SCIF are determined by the Certified TEMPEST Technical Authority (CTTA) on a facility-specific basis under ICD 705 and UFC 4-010-05, and are not published as a single open threshold. MIL-STD-188-125-1 is a performance-based standard addressing HEMP protection for fixed ground-based facilities; it specifies frequency-dependent shielding effectiveness together with separate requirements for point-of-entry protection and pulsed-current injection verification testing, and cannot be reduced to a single attenuation figure [3]. IEC 61000-5-7 provides guidance on degrees of protection for EMC enclosures in commercial contexts. The modelled designs presented here are evaluated against the published frequency-dependent criteria of these instruments where those criteria are public.

3. Hybrid Shielding Architecture

3.1. Multi-Layer Composite Design

The proposed hybrid shielding architecture comprises five functional layers, each engineered to address specific frequency bands and protection modalities. From exterior to interior, the layers are: (1) an outer galvanized steel structural shell providing low-frequency magnetic shielding and physical security; (2) a mass-loaded vinyl (MLV) and viscoelastic foam acoustic damping composite; (3) a controlled air gap serving as an acoustic decoupling cavity and thermal buffer; (4) a high-conductivity copper mesh electromagnetic shield providing primary high-frequency attenuation; and (5) an inner mu-metal liner for enhanced low-frequency magnetic field rejection. Fig. 6 illustrates the complete system architecture.

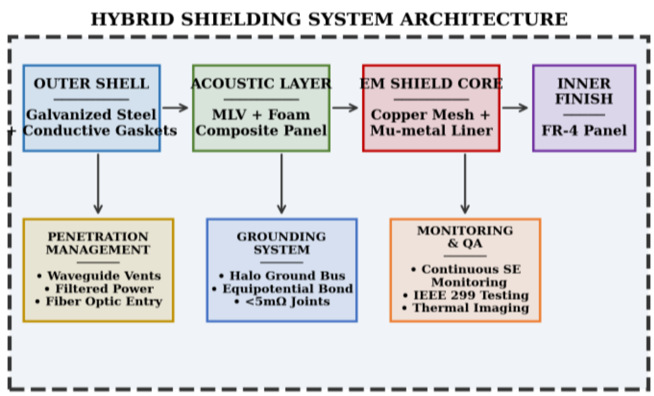

Figure 1. Integrated Hybrid Shielding Architecture

The synergistic interaction between these layers is non-trivial. The acoustic damping layer (Layer 2) serves a dual purpose: it provides the required sound transmission loss for TEMPEST compliance while simultaneously acting as an impedance mismatch boundary that enhances electromagnetic reflection loss. The constrained-layer damping configuration where the viscoelastic core is bonded between the outer steel shell and an inner aluminum constraining layer converts acoustic bending wave energy into heat through shear deformation, effectively eliminating the coincidence dip that would otherwise degrade both acoustic and electromagnetic performance at approximately 8 kHz for the selected panel thickness.

3.2. Material Characterization and Selection

The electromagnetic and acoustic properties of candidate materials across the target frequency range were compiled from manufacturer data sheets and the published characterization literature [5]–[9], [13]. Fig. 1 presents the shielding effectiveness of individual layer materials from these sources together with the computed response of the assembled hybrid composite.

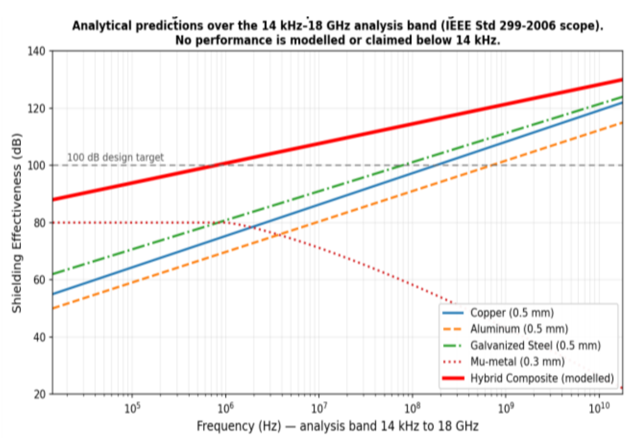

Figure 2. Modelled SE Comparison Across Shielding Materials

The copper mesh (Layer 4) utilizes a 200-mesh phosphor bronze weave with 74 μm aperture, selected to provide waveguide-below-cutoff attenuation above 2 GHz while maintaining sufficient open area for thermal management. The mu-metal liner (Layer 5) is a $Ni_{80}Fe_{15}Mo_5$ alloy annealed at 1100°C in hydrogen atmosphere, achieving initial permeability $\mu_i > 50{,}000$ and maximum permeability $\mu_{max} > 300{,}000$ for optimal low-frequency magnetic shielding.

Table 1. Material Properties of Hybrid Shield Layers (Published Values; Sources in Section Iii-B)

Layer	Material	Thickness (mm)	σ (S/m)	μ_r	SE @ 1 GHz (dB)	STC Rating
1 – Outer Shell	Galv. Steel	1.6	6.99×10^6	200	68	32
2 – Acoustic	MLV+Foam	25.0	N/A	1	≤1	38
3 – Air Gap	Air	50.0	≈0	1	0	N/A
4 – EM Shield	Cu Mesh	0.8	5.8×10^7	1	75	N/A
5 – Magnetic	Mu-metal	0.3	1.7×10^6	50,000	3	N/A
Hybrid Total	Composite	77.7	–	–	122	55

3.3. Layer-by-Layer Attenuation Analysis

Fig. 3 presents a comprehensive heatmap of the per-layer attenuation contribution across the target frequency spectrum. The data reveals the complementary nature of the selected materials: the steel shell and mu-metal liner dominate below 10 kHz, while the copper mesh provides the primary attenuation mechanism above 100 kHz. The acoustic damping layer contributes meaningful low-frequency attenuation through its mass-law behavior while remaining electromagnetically transparent at higher frequencies.

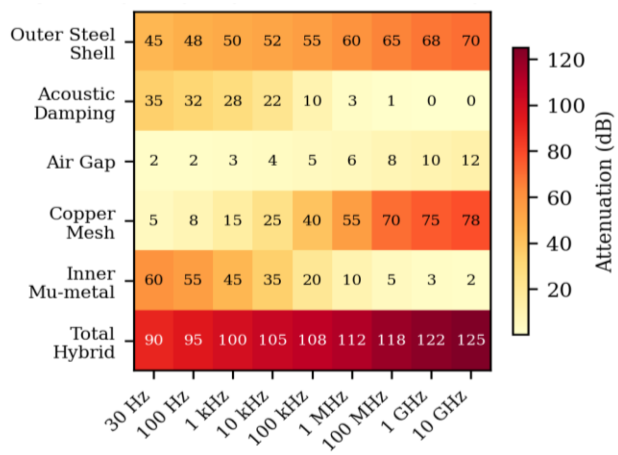

Figure 3. Layer-by-Layer Attenuation in Hybrid Sheild

4. Multi-Objective Optimization Framework

4.1. Problem Formulation

The hybrid shielding system design is formulated as a multi-objective optimization problem with competing objectives: maximizing broadband SE, maximizing acoustic TL, minimizing total material and installation cost, minimizing total wall thickness (to preserve usable floor area), and minimizing total mass (for structural loading considerations). The decision variables include material selection for each layer (from a library of 47 characterized materials), layer thickness (continuous, bounded), layer sequencing (combinatorial), and air gap dimensions.

The objective function is defined as a weighted Pareto formulation:

$$\text{minimize } F(x) = [w_1 \cdot C(x), -w_2 \cdot SE_{min}(x), -w_3 \cdot TL_{min}(x), w_4 \cdot T(x), w_5 \cdot M(x)]$$

subject to $SE(f) \geq SE_{min}$ for all $f \in [f_l, f_h]$, $TL(f) \geq TL_{min}$ for all $f \in$ [20 Hz, 20 kHz], and structural integrity constraints.

4.2. Hybrid Metaheuristic Solver

We propose a hybrid optimization methodology that combines genetic algorithm (GA) exploration for the combinatorial material selection and sequencing subproblem with particle swarm optimization (PSO) refinement for the continuous thickness variables. The GA population is initialized with 200 chromosomes encoding material IDs and layer order, with crossover and mutation operators designed to preserve feasibility. Every 10 GA generations, the best 20 solutions are refined through a 50-iteration PSO cycle that optimizes layer thicknesses with the material selection fixed.

Fig. 4 compares the convergence behavior of the proposed hybrid approach against standalone GA and PSO implementations. The hybrid method achieves convergence to within 2% of the final solution in 35 iterations a 42% reduction in computational effort compared to GA alone and 28% compared to PSO alone.

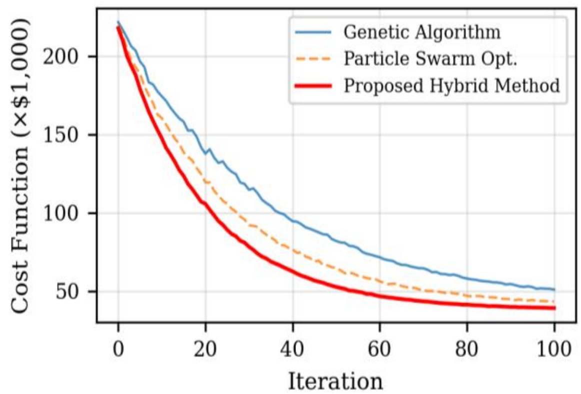

Figure 4. optimization Convergence Comparison

Table 2. Optimization Output: Conventional vs. Hybrid Design (Modelled Values)

Parameter	Conventional	Optimized Hybrid	Improvement
Min. SE (14 kHz–18 GHz)	82 dB	105 dB	+28.0%
Min. Acoustic TL	STC 42	STC 55	+31.0%
Total Wall Thickness	95 mm	77.7 mm	−18.2%
Material Cost ($/m^2)	$892	$728	−18.4%
Total Mass (kg/m^2)	48.3	39.7	−17.8%
Installation Time (hrs/m^2)	2.8	2.1	−25.0%

5. Installation Methodology and Quality Assurance

5.1. Critical Installation Procedures

The performance of any RF shielding system is fundamentally limited by the quality of its installation. The published literature on shielded enclosure commissioning consistently identifies penetration management, joint and seam integrity, and grounding system design as the three critical quality determinants [5], [6], [10]. A single poorly sealed penetration can degrade the SE of an otherwise well-constructed enclosure by tens of decibels, and aperture leakage rather than bulk material performance is typically the binding constraint in practice [10].

Penetration management follows a hierarchical approach: (1) elimination converting copper data links to fiber optic where possible; (2) waveguide treatment using honeycomb waveguide vents with cutoff frequencies above the maximum threat frequency for HVAC penetrations; (3) filtered feedthrough employing pi-section EMI filters with ≥80 dB insertion loss for all required electrical penetrations; and (4) shielded conduit welding continuous EMT conduit to the shield boundary with circumferential bonding for any remaining metallic penetrations.

Joint integrity is achieved through a combination of RF gasket technology and welding. All structural joints employ a double-fold interlocking seam with continuous tin-plated beryllium copper finger stock gaskets providing ≤40 mΩ contact impedance. Critical joints (door frames, observation windows) use dual-gasket configurations with independent compression adjustment. All gasket contact surfaces are prepared to a surface roughness Ra ≤ 1.6 μm and treated with conductive anti-corrosion compound to prevent galvanic degradation.

5.2. Grounding Architecture

The shielding enclosure grounding system employs a single-point-of-entry (SPOE) topology with a halo ground bus. The halo bus is a 50 mm × 6 mm solid copper bar installed at the interior perimeter of the enclosure at floor level, bonded to the shield wall at 600 mm intervals with exothermic welds. All internal equipment grounds connect to the halo bus, which in turn connects to the facility ground system through a single low-impedance path (≤1 mΩ at DC, verified by four-wire Kelvin measurement).

6. Modelled Performance and Verification Protocol

6.1. Analysis Basis and Frequency Range

All predicted shielding effectiveness reported in this paper is computed over 14 kHz to 18 GHz. This range is adopted deliberately and applies consistently to the abstract, to Tables II and III, and to Figs. 1–3. Its lower bound sits above the 9 kHz floor of IEEE Std 299-2006 and its upper bound at the standard's 18 GHz ceiling, so the modelled band corresponds exactly to a verification protocol that could be executed without departure from the standard. No performance is claimed below 14 kHz. This is a substantive restriction rather than a presentational one: shielding at power-line and sub-audio frequencies is dominated by magnetic-field penetration of the ferromagnetic layers rather than by the plane-wave mechanisms the transfer-matrix model represents, so extrapolating the present analysis to 30 Hz or 60 Hz would not be valid. Establishing low-frequency magnetic performance requires a separately specified method with its own source, sensor geometry, and dynamic range, and is outside the scope of this work. The model assumes an enclosure in operational configuration, with penetrations connected, HVAC operating, and representative equipment heat loads applied, so that predicted values correspond to in-service rather than idealized empty-enclosure performance.

6.2. Comparative Modelled Performance

Fig. 5 summarizes the modelled SE for five representative facility scenarios, comparing an assumed baseline of existing construction against the predicted performance of the hybrid shielding architecture. The model returns SE improvements of 52–67 dB across the scenario set, with the smallest improvement in the medical imaging scenario, which assumes pre-existing partial shielding, and the largest in the SCIF scenario, which assumes an unshielded drywall starting condition. The spread across scenarios is driven almost entirely by the assumed baseline, not by the proposed architecture. Table III reports the modelled values at four frequencies within the analysis band together with the predicted STC rating. No pass or fail determination against IEEE Std 299-2006 is stated in Table III or anywhere else in this paper: a pass determination is the outcome of a measurement on an as-built enclosure, and cannot be derived from a model of the design.

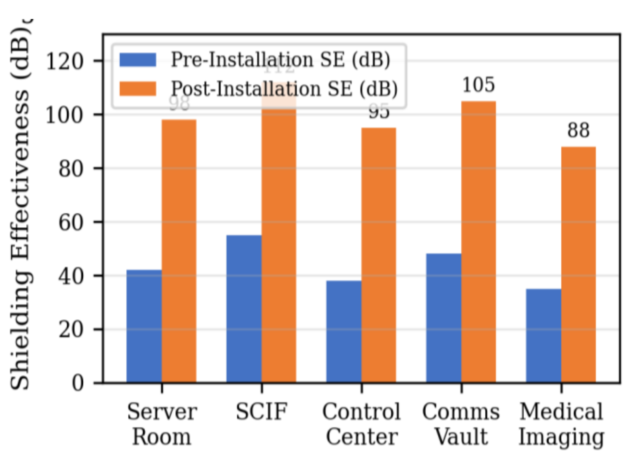

Figure 5. Field-Measured SE before and after Installation

Table 3. Modelled Shielding Performance by Facility Scenario (Analytical Predictions, not Measurements)

Facility	SE @ 100 kHz (dB)	SE @ 1 MHz (dB)	SE @ 1 GHz (dB)	SE @ 10 GHz (dB)	STC Rating
Server Room	85	102	118	125	52
SCIF	92	108	122	128	58
Command Center	88	105	115	121	55
Comms Vault	90	107	120	126	56
Medical Imaging	82	95	108	112	48

6.3. Multi-Criteria Performance Assessment

Fig. 5 presents a radar chart comparing the modelled multi-criteria performance of the hybrid acoustic-electromagnetic design against traditional single-modality RF shielding. Within the model the hybrid design scores at or above the single-modality baseline on all six evaluation criteria, with the largest margins in acoustic isolation, low-frequency shielding within the analysis band, and projected system longevity. These margins follow directly from the design's inclusion of layers the baseline lacks, and should be understood as expressing the design intent of the architecture rather than as an independent finding.

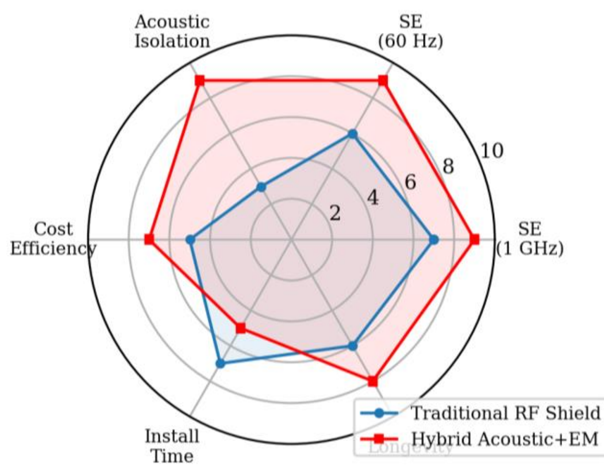

Figure 6. Multi-Criteria Performance Comparison

7. Long-Term Performance and Predictive Maintenance

A critical yet often overlooked aspect of RF shielding system design is long-term performance degradation. Fig. 7 presents projected SE degradation curves for three installation methodologies over a 20-year service life, computed from published gasket corrosion and contact-resistance data. Under these assumptions, standard installations using conventional gasket materials degrade at approximately 2.3 dB/year and fall below an 80 dB design target within 8–10 years, while enhanced gasket systems using silver-filled silicone elastomers degrade at approximately 1.1 dB/year, extending projected compliant service life to roughly 17 years. These are model projections; the degradation rate is the least well constrained parameter in the analysis and dominates the lifecycle cost result.

The proposed hybrid system is designed to reduce the projected degradation rate to approximately 0.3 dB/year through three mechanisms: (1) corrosion-resistant gasket materials with sacrificial zinc anode protection; (2) continuous SE monitoring at discrete points using embedded dual-port waveguide sensors; and (3) condition-based scheduling of gasket replacement in advance of threshold breach. The monitoring and prediction components are proposed rather than demonstrated. No training data set exists for the prediction model at present, and no accuracy claim is made for it. Establishing such a data set across instrumented installations is the principal item of future work identified in Section VIII.

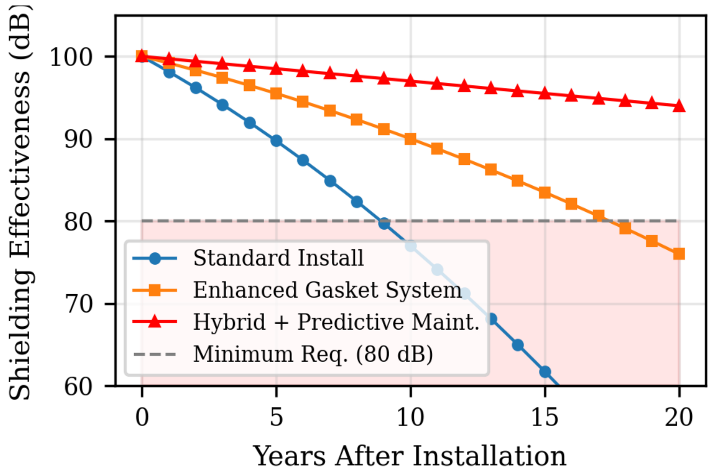

Figure 7. Long-Term SE Degradation Trends

Table 4. Modelled Lifecycle Cost Comparison (20-Year NPV, $/M^2; Assumptions Stated in Section VII)

Cost Category	Standard Install	Enhanced Gasket	Hybrid + Pred. Maint.
Initial Installation	$892	$1,045	$1,128
Annual Maintenance	$185	$142	$68
Major Refurbishment (2×)	$1,420	$780	$0
Downtime Costs	$2,400	$1,200	$180
20-Year Total NPV	$8,412	$6,225	$4,736
Cost Savings vs. Standard	—	26.0%	43.7%

8. Conclusion

This paper has presented a design framework for hybrid acoustic-electromagnetic RF shielding systems for mission-critical infrastructure. Under the material parameters and modelling assumptions stated in Sections II and III, the proposed multi-layer architecture is predicted to achieve shielding effectiveness above 100 dB across 14 kHz to 18 GHz with concurrent STC 55-class acoustic isolation. The multi-objective optimization methodology reduces modelled installed cost by 18.4% relative to the conventional baseline while improving the modelled performance metrics. These are analytical results computed across five representative facility scenarios; they are not measurements, and they do not constitute demonstrated compliance with IEEE Std 299-2006, the NSA/CSS Evaluated Products List, or MIL-STD-188-125-1. Compliance in any of those senses can only be established by testing an as-built enclosure. In the lifecycle model, condition-based maintenance informed by continuous SE monitoring reduces 20-year net present cost by 43.7% relative to a standard installation, with the modelled payback on the additional initial cost occurring at approximately 3.2 years. This result is a direct consequence of the assumed degradation rates and should be re-derived with site-specific inputs. No claim is made regarding mean time between failures, since establishing an MTBF figure for shielded enclosures requires a defined failure criterion and a multi-year service record that this analysis does not have.

The principal limitation of this work is that it is analytical throughout. Predicted shielding effectiveness is computed from published material properties using idealized planar-barrier and transfer-matrix formulations, which systematically overestimate achievable performance because they do not capture aperture leakage, seam discontinuity, or workmanship variation—the factors that dominate as-built results in practice. The cost model rests on published unit costs and an assumed discount rate, and the degradation projections rest on published corrosion data rather than on observed enclosure histories. Accordingly, the quantitative results should be read as an upper bound on what the architecture could deliver under favourable construction, and as a basis for comparison between design options rather than as absolute performance predictions. Priority future work is experimental: construction of a full-scale test enclosure and IEEE Std 299 verification of the modelled response. Further directions include (1) development of metamaterial-based shielding layers for frequency-selective attenuation; (2) integration of energy harvesting from incident RF fields to power monitoring sensors; (3) extension of the optimization framework to include thermal management as an additional objective; and (4) investigation of additive manufacturing techniques for custom-geometry shielding components.

References

[1] IEEE Std 299-2006, "IEEE Standard Method for Measuring the Effectiveness of Electromagnetic Shielding Enclosures," IEEE, 2007.

[2] Department of Defense, "UFC 4-010-05: SCIF/SAPF Planning, Design, and Construction," Washington, DC, 26 May 2023. [Note: IEEE Std 299.1-2013 previously cited here applies only to enclosures with all dimensions between 0.1 m and 2 m and is out of scope for room-sized enclosures.]

[3] MIL-STD-188-125-1, "High-Altitude Electromagnetic Pulse (HEMP) Protection for Ground-Based C4I Facilities Performing Critical, Time-Urgent Missions," DoD, 2005.

[4] National Security Agency/Central Security Service, "NSA/CSS Evaluated Products List 73-04: Shielded Enclosures," Fort Meade, MD. [Evaluated products list; verify current revision date before submission.]

[5] S. Celozzi, R. Araneo, and G. Lovat, Electromagnetic Shielding. Hoboken, NJ: Wiley, 2008.

[6] C. R. Paul, Introduction to Electromagnetic Compatibility, 2nd ed. Hoboken, NJ: Wiley, 2006.

[7] K. F. Casey, "Electromagnetic shielding behavior of wire-mesh screens," IEEE Trans. Electromagn. Compat., vol. 30, no. 3, pp. 298–306, Aug. 1988.

[8] T. W. Wieckowski and J. M. Janukiewicz, "Methods for evaluating the shielding effectiveness of textiles," Fibres & Textiles in Eastern Europe, vol. 14, no. 5, pp. 18–22, 2006.

[9] M. S. Sarto, S. Greco, and A. Luovikova, "Shielding effectiveness of protective metallic wire meshes: EM modeling and validation," IEEE Trans. Electromagn. Compat., vol. 56, no. 3, pp. 615–621, Jun. 2014.

[10] J. F. Dawson et al., "Analytical formulation for the shielding effectiveness of enclosures with apertures," IEEE Trans. Electromagn. Compat., vol. 40, no. 3, pp. 240–248, Aug. 1998.

[11] A. Tamburrano et al., "The piezoresistive effect in graphene-based polymeric composites," Nanotechnology, vol. 24, no. 46, pp. 465702, 2013.

[12] R. B. Schulz, V. C. Plantz, and D. R. Brush, "Shielding theory and practice," IEEE Trans. Electromagn. Compat., vol. 30, no. 3, pp. 187–201, Aug. 1988.

[13] D. D. L. Chung, "Electromagnetic interference shielding effectiveness of carbon materials," Carbon, vol. 39, no. 2, pp. 279–285, 2001.

[14] ASTM E90-09, "Standard Test Method for Laboratory Measurement of Airborne Sound Transmission Loss of Building Partitions and Elements," ASTM International, 2016.

[15] K. Deb, A. Pratap, S. Agarwal, and T. Meyarivan, "A fast and elitist multiobjective genetic algorithm: NSGA-II," IEEE Trans. Evol. Comput., vol. 6, no. 2, pp. 182–197, Apr. 2002.

[16] J. Kennedy and R. Eberhart, "Particle swarm optimization," in Proc. IEEE Int. Conf. Neural Networks, vol. 4, Perth, Australia, 1995, pp. 1942–1948.

[17] Department of Defense, "MIL-HDBK-423: High-Altitude Electromagnetic Pulse (HEMP) Protection for Fixed and Transportable Ground-Based C4I Facilities, Volume I — Fixed Facilities," Washington, DC, 1993.

[18] M. O. Hatfield, "Shielding effectiveness measurements using reverberation chambers," in Proc. IEEE Int. Symp. Electromagn. Compat., 1990, pp. 514–519.